Joint insolation and ice sheet/CO_2 forcing on northern China precipitation during Pliocene warmth

Zeng Luo[a], Junsheng Nie[a,b,*], Annelisa Ehret Moe[c], Richard V. Heermance[c], Carmala Garzione[d], Timothy D. Herbert[e], Zhao Wang[a], Hua Li[f], Rui Zhang[g], Xiangming Zhao[e], Ulrich Salzmann[h]

[a]*Key Laboratory of Western China's Environment System (Ministry of Education), Lanzhou University, Lanzhou 730000, China*

[b]*CAS Center for Excellence in Tibetan Plateau Earth Sciences, Chinese Academy of Sciences (CAS), Beijing 100101, China*

[c]*Department of Geological Sciences, California State University, Northridge 91330-8266, USA*

[d]*Department of Environmental Sciences, Rochester Institute of Technology, Rochester 14623, USA*

[e]*Department of Earth, Environmental, and Planetary Sciences, Brown University, Providence 02912, USA*

[f]*Department of Chemistry, Lanzhou University, Lanzhou 730000, China*

[g]*School of Geography, Geomatics and Planning, Jiangsu Normal University, Xuzhou 221116, China*

[h]*Department of Geography and Environmental Sciences, Northumbria University, Newcastle upon Tyne NE1 8ST, UK*

* Corresponding author. *E-mail address*: jnie@lzu.edu.cn (J. Nie)

East Asian summer monsoon (EASM) precipitation affects the lives of billions of people and impacts the stability of fragile desert ecosystems in central Asia [1]. Therefore, many studies have focused on understanding the variability of the EASM and its relationship with insolation, ice sheet, and CO_2 forcings [1-3]. Evidence for EASM variability is preserved in the eolian dust sequences on the Chinese Loess Plateau (CLP), which highlight the importance of Northern Hemisphere (NH) ice sheets, CO_2 levels, and insolation in controlling the strength of the EASM during the Quaternary [2]. In contrast, Pliocene (5.3-2.6 Ma) proxy records of the EASM from the CLP reveal weak orbital signals, suggesting weak sensitivity to ice sheets, CO_2 levels, and insolation forcing during this sustained warm period [4]. These Pliocene proxy records also contrast model simulations which suggest high sensitivity of the EASM to orbital forcing (particularly precession) during this time [5].

In order to investigate the apparent lack of strong orbital cycles in the Pliocene records from the CLP characterized by warm northern high latitudes and minor NH ice sheets [6], we generate a high-resolution (3 ka) monsoon precipitation record from the Loess Plateau (Fig. 1) using a recently proposed, promising magnetic parameter-based precipitation proxy (χ_{fd}/HIRM), with larger values corresponding to higher precipitation (see supplementary methods).

Using either established paleomagnetic age model of the Loess Plateau Chaona site (supplementary methods and Fig. S1) or the orbitally-tuned age model (supplementary methods and Fig. S2), the χ_{fd}/HIRM record consistently shows dominant 20-ka cycles, in sharp contrast with the loess magnetic susceptibility record from the same section

(Fig. 2 and Fig. S3), which fails to resolve any orbital cycles during the 3.25-2.95 Ma. The comparison of χ_{fd}/HIRM with June insolation gradient between 30^{o} N and 30^{o} S [7] suggests that high χ_{fd}/HIRM values align well with the high June insolation gradient (Fig. 2 and Fig. S3). We note that boreal summer insolation shows similar trends (Fig. S4) to the June insolation gradient (30^{o} N – 30^{o} S), but modern climate data suggest that the interhemispheric summer insolation gradient is a more likely forcing mechanism for monsoon moisture than boreal summer insolation [8].

Our results suggest that precipitation decreases at four low insolation intervals between 3.15 and 2.95 Ma (highlighted by pink bands, Fig. 2 and Fig. S3), although these decreases are not as pronounced as the other low insolation intervals, suggesting a non-linear response to insolation forcing. Interestingly, these four intervals correspond to larger ice volume (Fig. 2 and Fig. S3), indicating a likely role that ice sheets played in controlling monsoon precipitation. This inference is supported by comparing the 40-ka band variations, where precipitation is out-of-phase with the June insolation gradient (Fig. S5) but in-phase with the benthic oxygen isotope stack [9] (Fig. S2). The χ_{fd}/HIRM record also shows non-orbital periodicities, such as the 30-ka and semi-precessional signals associated with beats or harmonics of orbital cycles [10] (Fig. 2), confirming that precipitation on the Loess Plateau had a non-linear response to insolation forcing.

In order to test whether both insolation and ice sheets are joint forcing for northern China precipitation, we stacked the June insolation gradient with the benthic oxygen isotope record (Fig. S6). The stacked records show similar variations and cyclicities to the CLP precipitation proxy records, including main orbital cycles as well as semi-precessional cycles (Fig. S6), providing further support for the inference that both insolation and ice sheets are joint forcing for northern China precipitation variations during the middle Piacenzian.

Our results provide an opportunity to robustly understand precipitation variations in northern China and potential forcing during the Pliocene warmth at orbital bands. We discussed the implications of our findings as follows.

First, although the middle Piacenzian period is characterized by a stable warm climate, our record reveals that precipitation was highly sensitive to insolation forcing. This finding is consistent with the South China Sea K/Si-based monsoon record [11], and together, the marine and terrestrial records consistently reveal high sensitivity of precipitation to insolation forcing in sustained warm periods. Second, our record suggests that Antarctic ice sheets likely played an important role in affecting northern China precipitation. The benthic oxygen isotope stack should indicate global ice volume variations during the Quaternary after onset of intensive NH glaciations, with NH ice sheet size variations playing a key role [2]. During the warm Pliocene, however, before the intensive onset of NH glaciation, variations in the benthic oxygen isotope stack should mainly reflect Antarctica ice sheet variations. During this time, pollen evidence from a Russian Arctic lakes indicates late Pliocene summer temperatures up to 8ºC warmer than today, with mean temperature in the warmest month consistently above 10ºC, leaving little room for permanent ice sheets to exist [6]. Furthermore, drilling results from the Ross Sea reveal clear evidence for rapid cooling and Antarctica ice sheet size increase during the middle Piacenzian [12], supporting that middle

Piacenzian ice sheet variations mainly occurred in Antarctica. The link between Antarctic ice sheets and CLP precipitation, based on the in-phase relationship between precipitation and the benthic oxygen isotope stack at the 40-ka band, can be achieved by at least two processes. I) Model simulations suggest that larger Antarctic ice sheets can intensify upwelling of circum-Antarctica deep water, which can reduce Southern Hemisphere (SH) sea ice and warm surface seawater [13]. Subsequently, northward propagation of SH warm seawater can result in a warmer Eurasia, more water vapor transport from surrounding oceans to continental China, and a larger sea-land pressure gradient associated with an amplified sea-land thermal contrast [13]. All of these factors would be able to promote EASM precipitation increase. II) It has been proposed that larger Antarctic ice sheets tend to push the Mascarene high and Australia high northward to intensify cross-equatorial moisture transport and Asian monsoon precipitation [14]. We note, however, that Antarctic ice volume fluctuations in the Pliocene could be a symptom of an underlying global forcing from CO_2 amplification well known for the late Pleistocene [15]. Therefore, we consider both ice-volume and CO_2 to be important forcing mechanisms for the observed precipitation variations at the 40-ka band.

In summary, the χ_{fd}/HIRM data presented here provides a high-resolution proxy record of precipitation from northern China between 3.25-2.95 Ma. 20-ka (precessional) cycles dominate the record, challenging past research suggesting weak sensitivity of northern China precipitation to insolation forcing during this sustained warm period in the late Pliocene. In addition, this record suggests Antarctic ice sheet growth and/or global atmospheric CO_2 may influence precipitation at 40-ka timescales during this time. These findings highlight the importance of orbital forcing on precipitation even during times of relatively warm climate, such as the middle Piacenzian or during future climate scenarios.

Conflict of interest

The authors declare that they have no conflict of interest.

Acknowledgments

This manuscript benefits from constructive suggestions from four anonymous reviewers and the editors. This work was supported by Second Tibetan Plateau Scientific Expedition (grant 2019QZKK0704), and the National Natural Science Foundation of China (grants 42030505 and 41672157), and the State Scholarship Fund organized by the China Scholarship Council (CSC) in 2018, the Royal Society (IE 141128), and the U.S. National Science Foundation (Grant No. 1348005, 1348075, and 1545859).

Author contributions

Junsheng Nie designed the experiments. Zeng Luo, Rui Zhang and Zhao Wang performed experiments. All authors analyzed data. Junsheng Nie, Zeng Luo and Richard V. Heermance wrote the paper with the help of other authors.

References

[1] Cheng H, Edwards RL, Sinha A, et al. The Asian monsoon over the past 640,000 years and ice age terminations. Nature 2016; 534: 640-646.

[2] Hao QZ, Wang L, Oldfield F, et al. Delayed build-up of Arctic ice sheets during 400,000-year minima in insolation variability. Nature 2012; 490: 393-396.

[3] Wang YJ, Cheng H, Edwards RL, et al. Millennial- and orbital-scale changes in the East Asian monsoon over the past 224,000 years. Nature 2008; 451: 1090-1093.

[4] Sun YB, Clemens SC, An ZS, et al. Astronomical timescale and palaeoclimatic implication of stacked 3.6-Myr monsoon records from the Chinese Loess Plateau. Quat Sci Rev 2006; 25: 33-48.

[5] Yan Q, Zhang ZS, Zhang R. Investigating Sensitivity of East Asian Monsoon to Orbital Forcing During the Late Pliocene Warm Period. J Geophys Res 2018; 123: 7161-7178.

[6] Brigham-Grette J, Melles M, Minyuk P, et al. Pliocene warmth, polar amplification, and stepped Pleistocene cooling recorded in NE Arctic Russia. Science 2013; 340: 1421-1427.

[7] Laskar J, Robutel P, Joutel F, et al. A long-term numerical solution for the insolation quantities of the Earth. Astron Astrophys 2004; 428: 261-285.

[8] Beck JW, Zhou WJ, Li C, et al. A 550,000-year record of East Asian monsoon rainfall from ^{10}Be in loess. Science 2018; 360: 877-881.

[9] Lisiecki LE, Raymo ME. A Plio-Pleistocene stack of 57 globally distributed benthic d^{18}O records. Paleoceanography 2005; 20: PA1003.

[10] Thomas EK, Clemens SC, Sun YB, et al. Heterodynes dominate precipitation isotopes in the East Asian monsoon region, reflecting interaction of multiple climate factors. Earth Planet Sci Lett 2016; 455: 196-206.

[11] Wehausen R, Brumsack HJ. Astronomical forcing of the East Asian monsoon mirrored by the composition of Pliocene South China Sea sediments. Earth Planet Sci Lett 2002; 201: 621-636.

[12] McKay R, Naish T, Carter L, et al. Antarctic and Southern Ocean influences on Late Pliocene global cooling. Proc Natl Acad Sci 2012; 109: 6423-6428.

[13] Shi F, Yin QZ, Nikolova I, et al. Impacts of extremely asymmetrical polar ice sheets on the East Asian summer monsoon during the MIS-13 interglacial. Quat Sci Rev 2020; 230: 106164.

[14] An ZS, Clemens SC, Shen J, et al. Glacial-Interglacial Indian Summer Monsoon Dynamics. Science 2011; 333: 719-723.

[15] Lüthi D, Le Floch M, Bereiter B, et al. High-resolution carbon dioxide concentration record 650,000-800,000 years before present. Nature 2008; 453: 379-382.

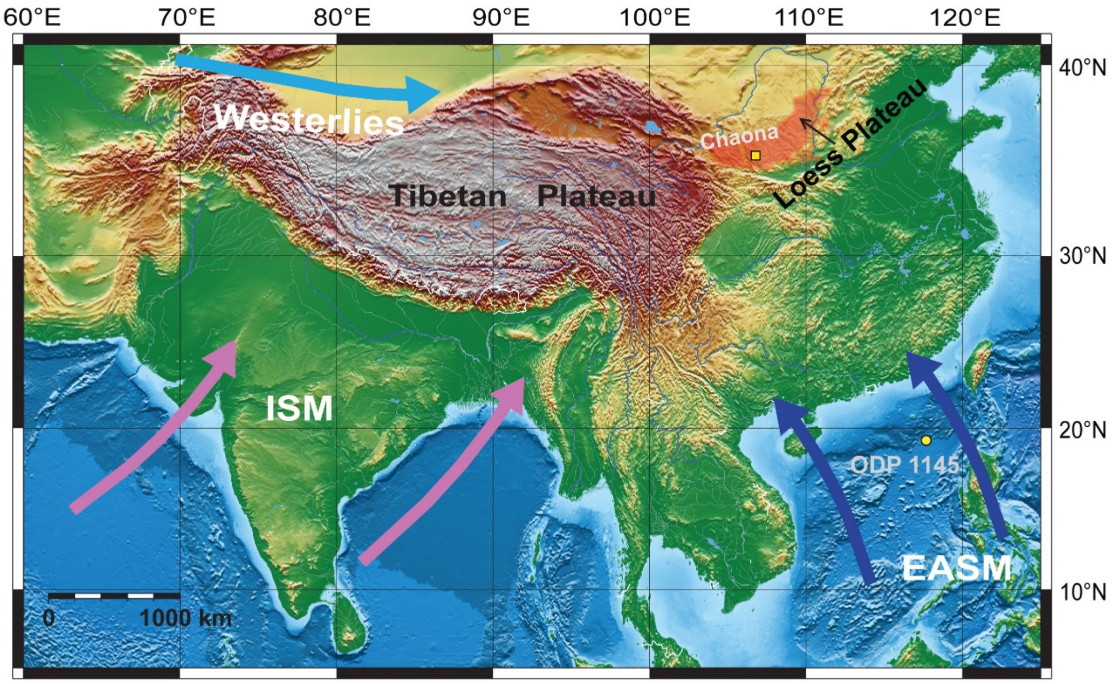

Fig. 1. Map of study sites and modern Asian summer atmospheric circulation pattern. EASM: East Asian summer monsoon. ISM: Indian summer monsoon.

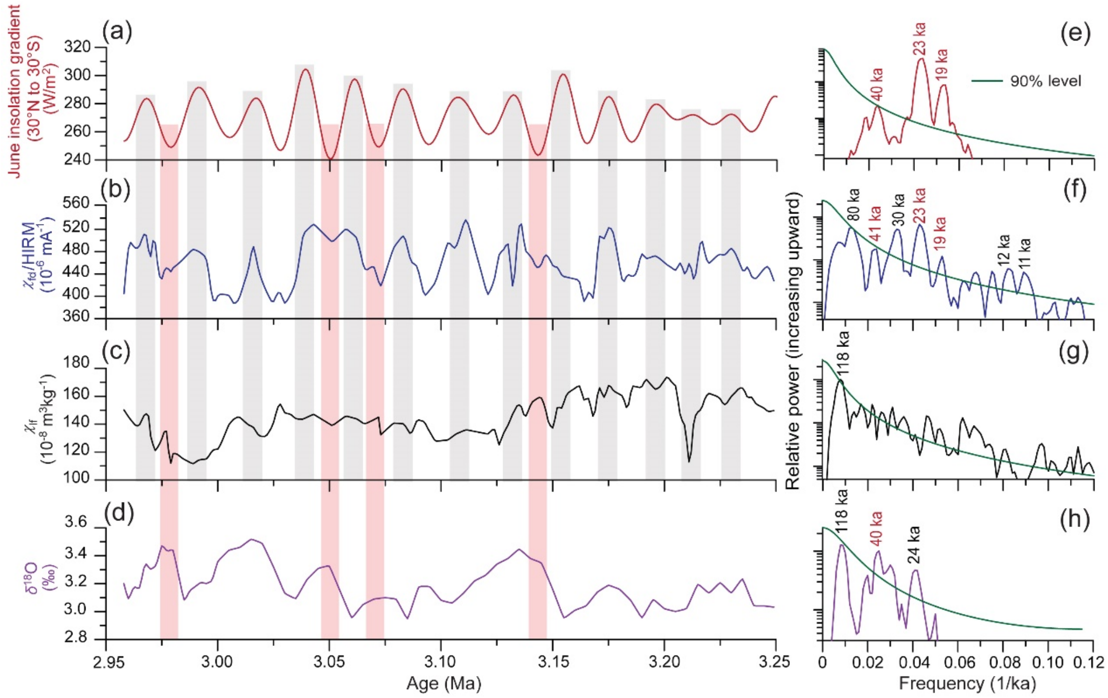

Fig. 2. Chaona paleoclimate records and comparison with June insolation gradient and benthic oxygen isotope stack. (a) June insolation gradient [7]. (b) Chaona χ_{fd}/HIRM. (c) Chaona χ_{lf}. (d) Benthic δ^{18}O stack [9]. (e)-(h) Power spectra of (a)-(d), respectively. The grey bands highlight the intervals where χ_{fd}/HIRM peaks correspond to June insolation gradient maxima. The pink bands highlight the complex relationship between χ_{fd}/HIRM, benthic δ^{18}O, and insolation gradient. The y axes of the spectral plots are in log 10 scale. The age model was based on orbital tuning.

Joint insolation and ice sheet/CO_2 forcing on northern China precipitation during Pliocene warmth

Zeng Luo, Junsheng Nie*, Annelisa Ehret Moe, Richard V. Heermance, Carmala Garzione, Timothy D. Herbert, Zhao Wang, Hua Li, Rui Zhang, Xiangming Zhao, Ulrich Salzmann

* Corresponding author. *E-mail address*: jnie@lzu.edu.cn (J. Nie)

This PDF file includes:

Abstract

Supplementary materials and methods

Supplementary figs. S1-S6

1. Abstract

The processes controlling East Asian summer monsoon (EASM) variations during past warm periods are poorly known but important for understanding its response to prolonged warming. The eolian dust sequences on the Chinese Loess Plateau (CLP) play a pivotal role in understanding EASM variations, revealing that Quaternary EASM was forced by joint ice sheets, CO_2 levels, and insolation forcing. However, the paleoclimate records from the Pliocene dust sequences on the CLP reveal weak sensitivity to any recognized forcing, which is inconsistent with model simulations. To resolve this puzzle, we present a 3-ka (thousand years) resolution precipitation record from the CLP, focusing on the middle Piacenzian (3.264–3.025 Ma), the closest persistently warm period in geological history, using a recently proposed precipitation proxy based on magnetic parameters. The record reveals dominant 20-ka precessional cycles, invalidating the prior hypothesis of a weak EASM sensitivity to insolation forcing during the warm Pliocene. At the 40-ka band, the precipitation record shows an inverse phase relationship with middle latitude summer insolation but an in-phase relationship with Southern Hemisphere ice volume, which we attribute to CO_2 and/or ice sheet control on northern China precipitation via atmosphere or marine processes. These findings demonstrate a strong and highly variable EASM during the Pliocene, reshaping our understanding of EASM variations in past warm periods.

2. Materials and methods

2.1. Magnetic proxy

Magnetic minerals produced during weathering are sensitive to climate in arid-semi arid region [16-19]. Hematite and nanometer-scale ferrimagnetic mineral (magnetite, which is quickly oxidized to maghemite due to high surface to volume ratio) are two commonly produced minerals during weathering [16, 19, 20]. It is generally accepted that hematite forms in dry environment [20]. In comparison with hematite, weathering-produced nanometer-scale magnetite requires periods of reducing conditions in sediment so that Fe^{3+} can be reduced to Fe^{2+}, which requires a wetter climate and higher precipitation [16, 21]. Therefore, the ratio of nanometer-scale magnetite-maghemite over hematite (i.e., the content of magnetic minerals generated during wetter climate divided by those generated during drier climate) is more sensitive to precipitation variations in the arid-semi arid regions than any single magnetic mineral alone. The ratio is represented by frequency-dependent magnetic susceptibility (χ_{fd})/hard isothermal remanent magnetization (HIRM), where χ_{fd} indicates content of pedogenic nanometer-scale ferrimagnetic grains and HIRM reflects hematite content.

In order to measure the χ_{fd}/HIRM values, 108 bulk samples were collected at 5 cm intervals in the Chaona section. We measured the magnetic susceptibility (χ) of these samples at a lower frequency of 976 Hz and a higher frequency of 15616 Hz, using the AGICO multi-function spinner Kappabridge (MFK1-FA). χ_{fd} was then calculated based on the equation of $\chi_{fd}=\chi_{976Hz}-\chi_{15616Hz}$. Isothermal remanent magnetization (IRM) intensity was measured at a magnetic field of 1.2 T and -0.3 T, respectively. HIRM (hard IRM) was calculated as $(IRM_{1.2T} + IRM_{-0.3T})/2$. Finally, we calculated χ_{fd}/HIRM values of 108 samples. These experiments were carried out at the Paleomagnetism Laboratory in the China University of Geosciences, Beijing, China.

2.2. Establishing the initial age model of the Chaona section on the Loess Plateau

The age model of the Chaona section (35.1°N, 107.2°E) on the CLP was established using paleomagnetism dating [22] in 2001. To reconstruct the orbital timescale precipitation variations of the middle Piacenzian, we collected bulk samples at 5 cm intervals for magnetic susceptibility analysis in September 2014. The good match between new magnetic susceptibility data and previous magnetic susceptibility data [22] in the Chaona section provides the age control points for establishing the age model of resampling Chaona section (Fig. S1). Based on the 8 age control points, we obtain the initial age model of new magnetic susceptibility data through piecewise linear interpolation.

2.3. Establishing the orbitally-tuned age model for the Chaona sections

The strong 20-ka cycles in the χ_{fd}/HIRM record and the similar pattern with insolation provide an opportunity to improve the precision of the age model from each section (Fig. S3f). Only minimal tuning was needed for each section (Fig. S2b). We note that the observed precipitation cyclicities and their comparison with insolation and ice sheet records are consistent between the paleomagnetic age model and the tuned age model (Fig. S2), indicating that tuning does not influence the results.

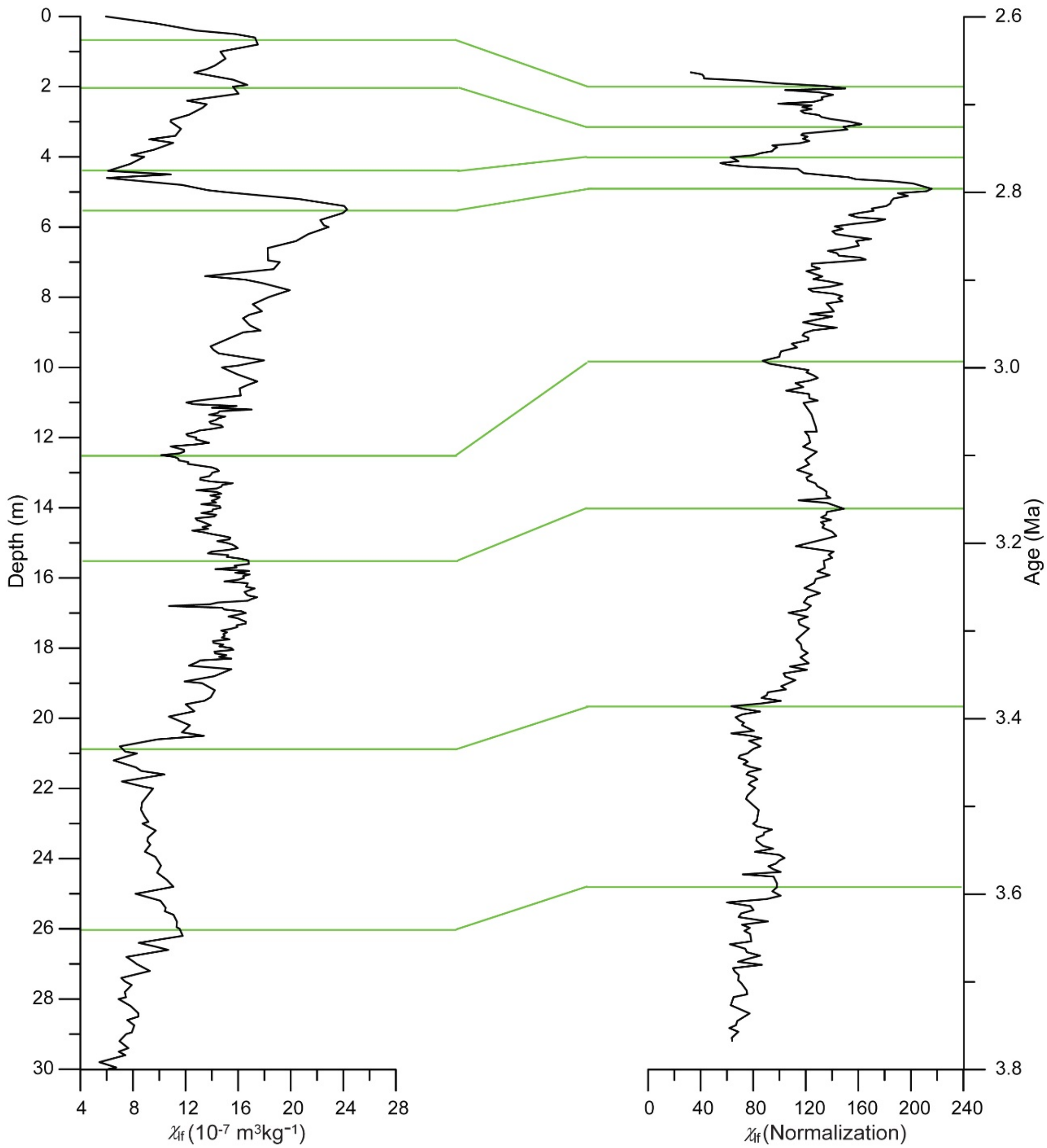

Fig. S1. The age control points for tuning the Chaona magnetic susceptibility. The right side is the new Chaona magnetic susceptibility data with depth and the left side is the previous Chaona magnetic susceptibility with age model [22]. χ_{lf}: Magnetic susceptibility at low frequency.

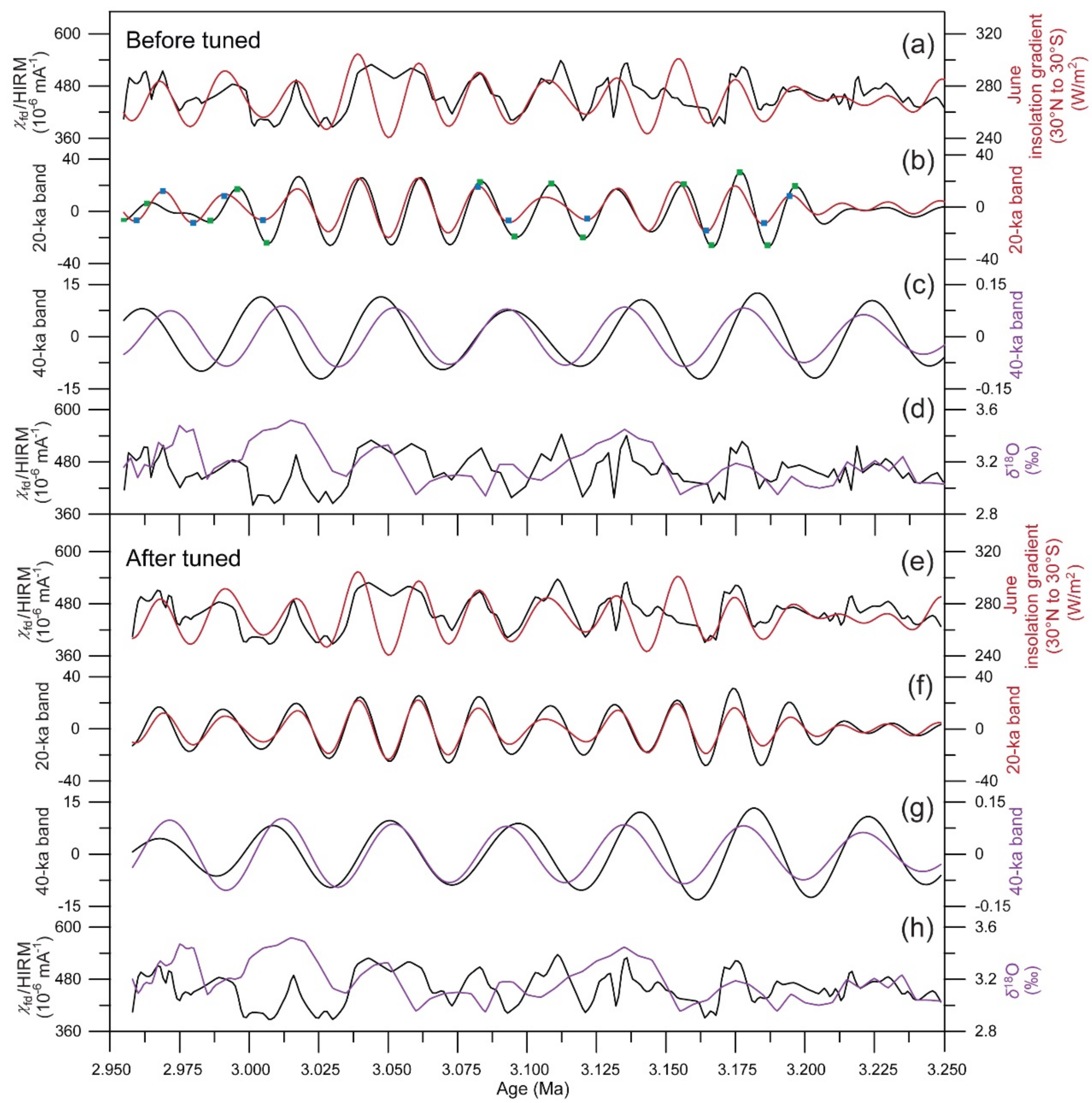

Fig. S2. A comparison of Chaona precipitation proxy record with June insolation gradient and benthic oxygen isotope stack. (a) and (e) χ_{fd}/HIRM and June insolation gradient [7]. (b**)** and (f) χ_{fd}/HIRM and June insolation gradient at filtered 20-ka band. (c) and (g) χ_{fd}/HIRM and benthic δ^{18}O stack [9] at filtered 40-ka band. (d**)** and (h) χ_{fd}/HIRM and benthic δ^{18}O stack. (b) show how the orbital tuning was done for Chaona section: green points in (b) were tuned to the closest insolation reference points (blue points). (a), (b), (c) and (d) show the results before tuned and (e), (f), (g) and (h) show the results after tuned. The 20-ka central frequency = 0.05 ka^{-1} and bandwidth = 0.012 ka^{-1}. The 40-ka central frequency = 0.024 ka^{-1} and bandwidth = 0.004 ka^{-1}.

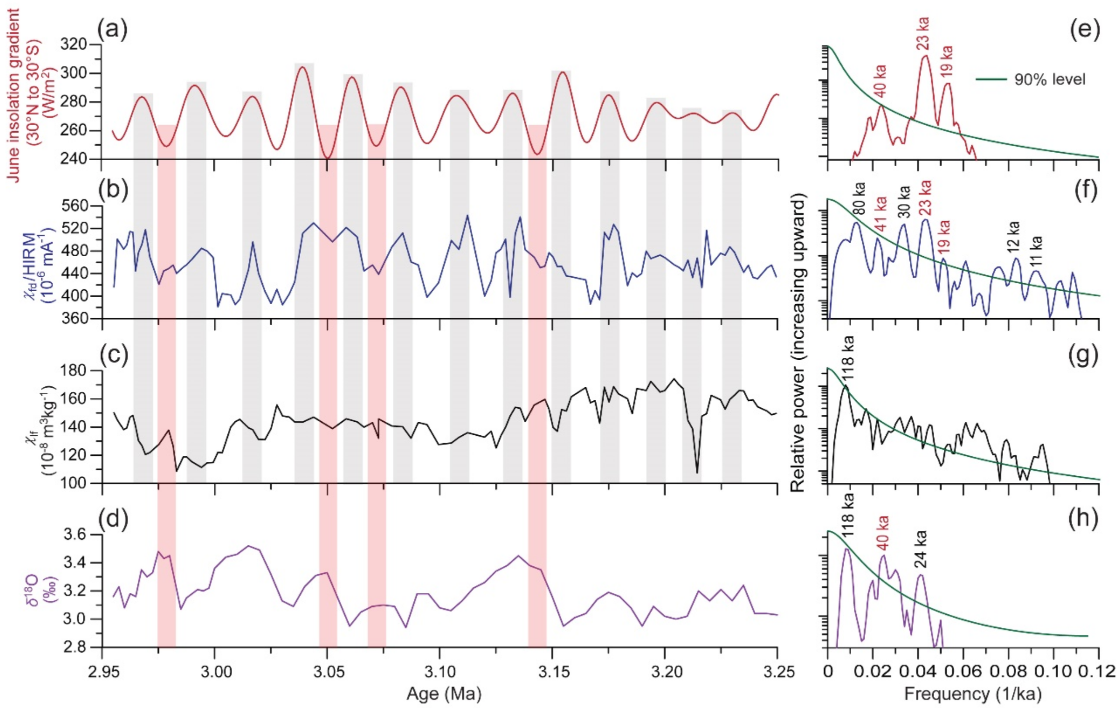

Fig. S3. Chaona paleoclimate records and comparison with June insolation gradient and benthic oxygen isotope stack based on paleomagnetic dating. (a) June insolation gradient [7]. (b) Chaona χ_{fd}/HIRM. (c) Chaona χ_{lf}. (d) Benthic $\delta^{18}O$ stack [9]. (e)-(h) Power spectra of (a)-(d), respectively. The grey bands highlight the intervals where χ_{fd}/HIRM peaks correspond to June insolation gradient maxima. The pink bands highlight the complex relationship between χ_{fd}/HIRM, benthic $\delta^{18}O$, and insolation gradient. The y axes of the spectral plots are in log 10 scale.

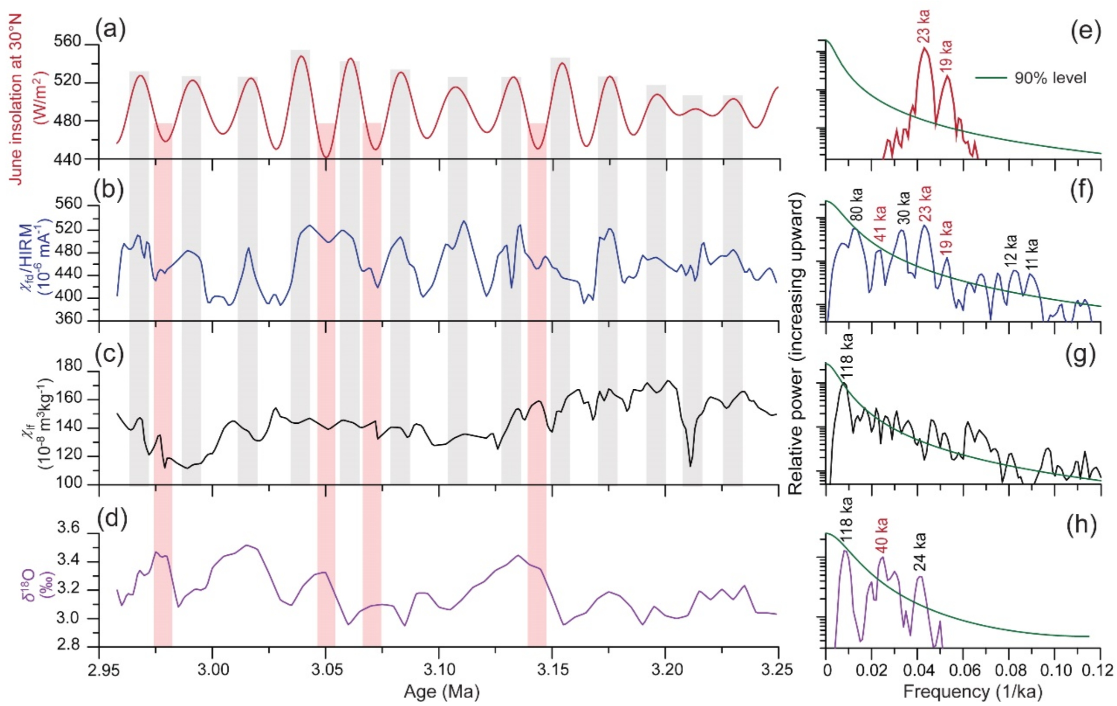

Fig. S4. Chaona paleoclimate records and comparison with June insolation at 30°N and benthic oxygen isotope stack based on orbitally-tuned age model. (a) June insolation at 30°N [7]. (b) Chaona χ_{fd}/HIRM. (c) Chaona χ_{lf}.. (d) Benthic δ^{18}O stack [9]. (e)-(h) Power spectra of (a)-(d), respectively. The grey bands highlight the intervals where χ_{fd}/HIRM peaks correspond to June insolation maxima. The pink bands highlight the complex relationship between χ_{fd}/HIRM, benthic δ^{18}O, and June insolation at 30°N. The y axes of the spectral plots are in log 10 scale.

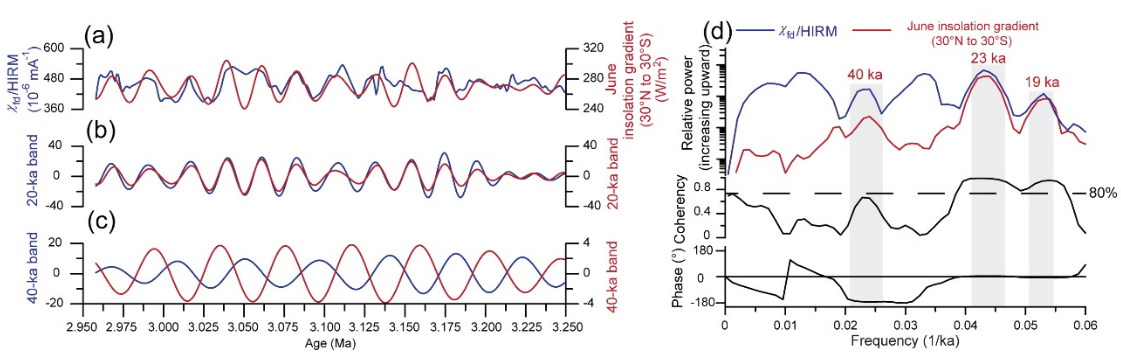

Fig. S5. Comparison of χ_{fd}/HIRM from Chaona section with June insolation gradient and their cross-spectral results based on orbitally-tuned age model. (a)-(c) Comparison of χ_{fd}/HIRM from Chaona section with June insolation gradient [7] and their filtered results at 20-ka and 40-ka bands. (d) Cross-spectral comparison of χ_{fd}/HIRM and June insolation gradient. The power spectral is plotted on log scale. The coherence is plotted on an arctanh scale (80% = 0.749). The grey bands show the dominant orbital cycles. At the 40-ka band, χ_{fd}/HIRM and June insolation gradient are out of phase. This cross-spectral analysis was based on ARAND Time-Series Analysis Software [23]. The 20-ka central frequency = 0.05 ka^{-1} and bandwidth = 0.012 ka^{-1}. The 40-ka central frequency = 0.024 ka^{-1} and bandwidth = 0.004 ka^{-1}.

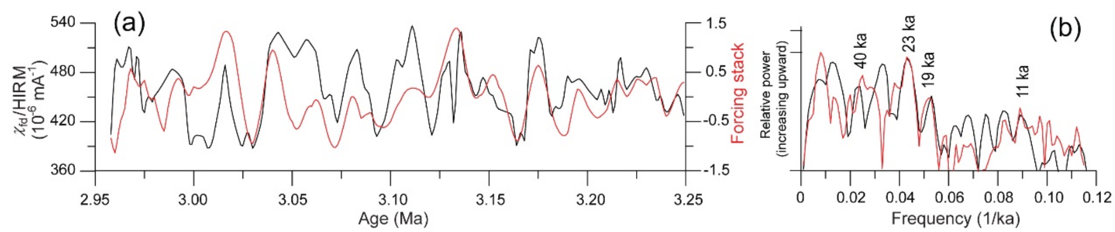

Fig. S6. Comparison of Loess Plateau χ_{fd}/HIRM with hypothesized insolation and ice sheet forcing stack based on orbitally-tuned age model. To produce the hypothesized forcing stack, we first normalized the June insolation gradient record and the benthic oxygen isotope record, then we multiplied the normalized benthic oxygen isotope record by 1.2 and added it with the normalized insolation record (hereafter forcing stack). (a) Comparison of Chaona χ_{fd}/HIRM with forcing stack. (c) The power spectral of (a), respectively. The y axes of the spectral plots are in log 10 scale.

References

[16] Liu ZF, Liu QS, Torrent J, et al. Testing the magnetic proxy χ_{FD}/HIRM for quantifying paleoprecipitation in modern soil profiles from Shaanxi Province, China. Global Planet Change 2013; 110: 368-378.

[17] King JW, Channell JET. Sedimentary magnetism, environmental magnetism, and magnetostratigraphy, 1987-1990. Rev Geophys 1991; 39: 358-370.

[18] Liu QS, Roberts AP, Larrasoana JC, et al. Environmental magnetism: principles and applications. Rev Geophys 2012; 50: RG4002.

[19] Verosub KL, Roberts AP. Environmental magnetism: Past, present, and future. J Geophys Res 1995; 100: 2175-2192.

[20] Schwertmann U, Taylor RM. Iron oxides. Minerals in Soil Environments, ed Dixon JB, Weed, S.B. Madison: Soil Science Society of America; 1987.

[21] Nie JS, Garzione C, Su QD, et al. Dominant 100,000-year precipitation cyclicity in a late Miocene lake from Northeast Tibet. Sci Adv 2017; 3: e1600762.

[22] Song YG, Fang XM, Li JJ, et al. The Late Cenozoic uplift of the Liupan Shan, China. Sci Chin (D) supp 2001; 44: 176-184.

[23] Howell P, Pisias N, Ballance J, et al. ARAND Time-Series Analysis Software. Brown University, Providence RI; 2006.